Research Article | Vol. 27, No. 13 | 24 Jun 2019 | OPTICS EXPRESS 17648
Optics EXPRESS

S-parameters, non-Hermitian ports and the finite-element implementation in photonic devices with $\mathcal{PT}$-symmetry

BEI WU,[1,3] ZHUORAN WANG,[1,3] WEIJIN CHEN,[1] ZHONGFEI XIONG,[1] JING XU,[1,2,4] AND YUNTIAN CHEN[1,2,5]

[1] *School of Optical and Electronic Information, Huazhong University of Science and Technology, Wuhan, China*
[2] *Wuhan National Laboratory for Optoelectronics, Huazhong University of Science and Technology, Wuhan, China*
[3] *These two authors contributed equally to this work*
[4] *jing_xu@hust.edu.cn*
[5] *yuntian@hust.edu.cn*

Abstract: In Hermitian photonic devices, S-parameters, i.e., the elements of a scattering matrix based on integrated power flux and Hermitian modal orthogonality, are used to account for the transmission or reflection of light from one port to another. The definition of S-parameters in Hermitian settings becomes inappropriate in the non-Hermitian optical environment. Here we revisit the fundamental problems associated with extracting the S-parameters of light in photonic $\mathcal{PT}$-symmetric devices, i.e., waveguides or coupled waveguide-cavity systems, wherein the waveguide ports themselves may also be non-Hermitian. We first use the bi-orthogonal inner product that restores the modal orthogonality on the waveguide ports containing balanced gain and losses to quantify the modal overlapping instead of Hermitian inner product. Secondly, a finite element implementation is proposed and realized to extract the S-parameters on non-Hermitian ports. Lastly, we illustrate our approach of calculating the S-parameters on non-Hermitian ports via two waveguide-lattice structures. The numerical results of S-parameters are validated against the constraints imposed by reciprocity and $\mathcal{PT}$-symmetry.

1. Introduction

S-parameters in electrical engineering describe the electrical behavior of linear electrical networks when undergoing various steady state stimuli by electrical signals. The network concept of circuit under long wavelength approximation can be extended to microwave and optics regime [1], and provides intuitive ideas of the circuit analysis for the coupled photonic devices. To apply the idea of circuit concept, i.e., using scattering matrix to describe the light flow in photonic devices, the key is to define the appropriate channels funnelling the optical power flux in and out [2]. Usually, those channels are taken as different optical modes, i.e., either bounded in waveguides or freely propagating in free space, which form an orthogonal and complete modal basis in Hermitian photonic devices.

Considering recent development in non-Hermitian photonics [3,4], $\mathcal{PT}$-symmetry in particular [5–11], it is natural to ask: (1) can the circuit concept be extended to non-Hermitian photonic devices connected to waveguide channels? (2) and can the connected waveguide channels which guide the light flow in/out the photonic devices themselves be non-Hermitian? The answer to the first question is positive as evident by the recent work of Ge and many others on the scattering properties of $\mathcal{PT}$ symmetric system. It is found out that the coherent perfect absorber (CPA) and $\mathcal{PT}$ laser absorber utilize the eigenvalues of scattering matrix corresponding to poles and zeros [12, 13], and the condition of corresponding singular blocks in the scattering matrix is

#361604 https://doi.org/10.1364/OE.27.017648
Journal © 2019 Received 5 Mar 2019; revised 9 May 2019; accepted 20 May 2019; published 12 Jun 2019

Optics EXPRESS

utilized to identify perfect transmission [14]. Moreover, S-parameters also play a crucial role in studying the topological properties of exceptional points (EPs) in $\mathcal{PT}$ symmetric systems [15, 16].

However, to the best of our knowledge, the second question associated with non-Hermitian waveguide channels (coined as non-Hermitian ports onward) and its numerical implementation is yet largely open to answer. The difficulty essentially lies in the failure of the Hermitian modal orthogonality in those non-Hermitian ports. To solve this problem, Zhang et. al [16] construct left-eigenmodes, which are orthogonal to both right-eigenmodes, via non-orthogonal right eigenmodes. The transmission coefficients can be then obtained by projecting the transverse field onto the left-eigenmodes. As the number of modes on the ports is larger than 2, the construction of left-eigenmodes is extremely complicated. Thus, it is desirable to develop an easy-to-implement method to obtain scattering matrix associated with non-Hermitian ports.

In this paper, we attempt to address the scattering properties of photonic devices connected with non-Hermitian ports. With the assistance of bi-orthogonal inner product, we restore the modal orthogonality in non-Hermitian ports, which can subsequently be used in the modal expansion for the extraction of S-parameters either analytically or numerically. We further propose a finite element implementation of the non-Hermitian port, emphasizing on its numerical realization on the boundaries.

This paper is organized as follows. In Section 2, we develop the basic concepts and principles in non-Hermitian ports, and then describe how the non-Hermitian port is accompanied with orthogonal modal functions under the bi-orthogonal inner product, and implemented in finite element calculations. In Section 3, we calculate S-parameters of two concrete examples in waveguide lattice from non-Hermitian ports using the aforementioned method, which is further verified by the constraints imposed by reciprocity and $\mathcal{PT}$- symmetry. Finally, Section 4 concludes the paper.

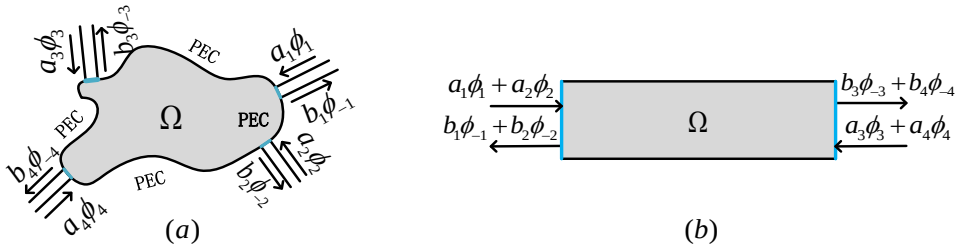

Fig. 1. (a) Schematic diagram of light scattering of a photonic device connected with a few waveguide channels indicated by the light blue segments S. The field inside the waveguide channel S is given by $\boldsymbol{\phi} = [\boldsymbol{e}^t \ \boldsymbol{h}^t]$. (b) Parallel plate waveguide. The light blue segments represent the waveguide channels, ϕ_1 and ϕ_2 are eigenmodes on the left boundary, while ϕ_3 and ϕ_4 are eigenmodes on the right boundary.

2. Principles in non-Hermitian port

2.1. Basic concepts in Hermitian port: scattering matrix, modal orthogonality and energy conversation

For self-consistency, we first introduce the basic concepts associated with Hermitian ports, i.e., scattering matrix, modal orthogonality as well as the conserved physical quantity, the counterparts of which in non-Hermitian settings will be discussed shortly. As an example of circuit analysis shown in Fig. 1(a), a photonic device is enclosed by fictitious boundary with 4 openings, each of which is connected with photonic waveguides. Light propagating in these waveguide channels

Optics EXPRESS

are given by the superposition of the eigen-solutions of Maxwell's equations,

$$\boldsymbol{E}_{\mu}^{t}(x,y,z) = (a_{\mu}e^{-i\beta_{\mu}z} + b_{\mu}e^{i\beta_{\mu}z})\boldsymbol{e}_{\mu}^{t}(x,y), \tag{1}$$

where a_μ is the complex amplitude of the light wave entering the photonic structure, b_μ is the complex amplitude of the wave propagating in the reverse direction (leaving the photonic device), μ is the mode label, and β_μ is the propagation constant. In consistency, the magnetic field is $\boldsymbol{H}_{\mu}^{t}(x,y,z) = (a_{\mu}e^{-i\beta_{\mu}z} - b_{\mu}e^{i\beta_{\mu}z})\boldsymbol{h}_{\mu}^{t}(x,y)$. In general, the different modal structures in those photonic waveguides are taken as different energy channels (ports that may or may not be overlapped in real space), in contrast to the separate ports in electrical network. Without mention, we assume there is one-to-one correspondence between one port and one in-coming or out-going wave. The modal fields of different ports are orthogonal if the scattering inside the boundary $\partial\Omega$ does not occur regardless of the physical overlapping of the modal field in real space. If the scattering inside the boundary $\partial\Omega$ indeed occurs (usually true), the field overlapping between the modes belonging to different ports is not necessarily zero, which is reflected by the non-zero elements in the scattering matrix. If different modal fields associated with different ports share the same cross section, such as two orthogonal modes propagating along a multimode waveguide, it is relevant to keep the exact modal orthogonality in extracting the scattering matrix.

In Hermitian photonic system, the Hermitian inner product is defined to characterize the mode orthogonality as follows, $\langle \boldsymbol{\psi}, \boldsymbol{\phi} \rangle = \int \boldsymbol{\psi}^{\dagger}\boldsymbol{\phi} d\Omega$, where $\boldsymbol{\phi}$ and $\boldsymbol{\psi}$ are the vector field containing electric field components and magnetic field components. Therefore, the mode orthogonality can be explicitly expressed as follows,

$$P\delta_{ij} = \iint \boldsymbol{e}_{i}^{t} \times \boldsymbol{h}_{j}^{t*} + \boldsymbol{e}_{j}^{t*} \times \boldsymbol{h}_{i}^{t} dxdy, \tag{2}$$

With projection onto the orthogonal modes associated with different ports, the in-coming/out-going waves can be given by A and B as column vectors. For linear, time-independent and passive photonic devices, the out-going/in-coming waves are connected by $\boldsymbol{B} = \bar{\boldsymbol{S}}\boldsymbol{A}$, where $\bar{\boldsymbol{S}}$ is the scattering matrix. The diagonal elements of $\bar{\boldsymbol{S}}$ are the reflection coefficients into backward propagating modes, whereas off-diagonal component S_{ij} denotes the transmission to port i with excitation imposed on port j. In Hermitian photonic devices, the total power of the out-going waves shall be equal to total incident power, which leads to the conservation relation of the scattering matrix as follows [17, 18],

$$\bar{\boldsymbol{S}}^{\dagger}\bar{\boldsymbol{S}} = \bar{\boldsymbol{I}}, \tag{3}$$

where † represents the Hermitian transpose of $\bar{\boldsymbol{S}}$.

2.2. Modal orthogonality in non-Hermitian port

In photonic devices with non-Hermitian ports, the aforementioned relation in Hermitian setting, i.e., the Hermitian modal orthogonality as well as conserved power flux are not valid. It is our intention to address this problem in $\mathcal{PT}$ symmetric devices, where the Hermitian modal orthogonality and power conservation need to be restored. In our previous work, we prove that the waveguide problem can be reformulated as a generalized eigenvalue problem determined by $(\bar{\boldsymbol{L}}, \bar{\boldsymbol{B}})$, i.e., $\bar{\boldsymbol{L}}\boldsymbol{\phi} = \beta\bar{\boldsymbol{B}}\boldsymbol{\phi}$, see more details in Chen's work [19]. Interestingly, we further show that the waveguide reciprocity, i.e., $(\boldsymbol{\psi}, \bar{\boldsymbol{L}}\boldsymbol{\phi}) = (\bar{\boldsymbol{L}}\boldsymbol{\psi}, \boldsymbol{\phi})$, under bi-orthogonal inner product requires that the materials of the waveguides are reciprocal ($\bar{\boldsymbol{\epsilon}}_r = \bar{\boldsymbol{\epsilon}}_r^T$, $\bar{\boldsymbol{\mu}}_r = \bar{\boldsymbol{\mu}}_r^T$). Importantly, the waveguide reciprocity can be reformulated into modal orthogonal relation as given by

$$(\beta_{\phi} - \beta_{\psi}) \langle \boldsymbol{\psi}, \boldsymbol{\phi} \rangle = (\beta_{\phi} - \beta_{\psi}) \int \boldsymbol{\psi}^{T}\bar{\boldsymbol{B}}\boldsymbol{\phi} d\Omega = 0, \tag{4}$$

Optics EXPRESS

where β_ϕ (β_ψ) is the propagation constant(eigenvalue) associated with mode $\boldsymbol{\phi}$ ($\boldsymbol{\psi}$). It is worthy to point out that physically the modes $\boldsymbol{\phi}$ and $\boldsymbol{\psi}$ usually can be taken as the forward and backward propagating modes. Explicitly, the mode orthogonality under bi-orthogonal inner product, $P\delta_{ij} = \iint dxdy\boldsymbol{\psi}_j^T \bar{\boldsymbol{B}}\boldsymbol{\phi}_i$ [20], can be given in terms of forward and backward propagating modes,

$$P\delta_{ij} = \iint \boldsymbol{e}_{\psi_i}^t \times \boldsymbol{h}_{\phi_j}^t - \boldsymbol{e}_{\phi_j}^t \times \boldsymbol{h}_{\psi_i}^t dxdy, \tag{5}$$

where $\boldsymbol{e}_\phi/\boldsymbol{h}_\phi$ ($\boldsymbol{e}_\psi/\boldsymbol{h}_\psi$) is the electric/magnetic field associated with mode $\boldsymbol{\phi}$ ($\boldsymbol{\psi}$). Notably, Eq. (5) has the physical meaning of un-conjugated form of Poynting vector along the propagation direction [21]. For the convenience of calculation, $\boldsymbol{\phi}$ and $\boldsymbol{\psi}$ are usually linked by additional symmetry. For Hermitian situation, where time reversal symmetry exists, the relation between forward propagating mode and backward propagating mode is $\boldsymbol{\psi} = \bar{\boldsymbol{\sigma}}\boldsymbol{\phi}^*$, where $\bar{\boldsymbol{\sigma}}$=diag[1 1 -1 -1], which reverse the sign of transverse magnetic field while the transverse electric field remains unchanged [22]. However for the non-Hermitian port with presence of gain and losses, the time reversal symmetry does not apply. In contrast, the chiral symmetry is still valid, from which the backward propagating mode can be expressed as $\boldsymbol{\psi} = \bar{\boldsymbol{\sigma}}\boldsymbol{\phi}$ [22]. Thus, Eq. (5) provides a convenient procedure of calculating the normalization factor in the numerical extraction of scattering matrix in our non-Hermitian ports. The normalized modal field is given by $\widetilde{\boldsymbol{\phi}} = \sqrt{\frac{P_{in}}{P}}\boldsymbol{\phi}$, where P is calculated using Eq. (5) and P_{in} is the integrated power flux of the incident mode.

2.3. Numerical considerations in FEM

We proceed to discuss the practical implementations of non-Hermitian port in FEM, which are realized in a commercial software package: COMSOL MULTIPHYSICS [23]. A typical finite element calculation of scattering problem is to impose the excitation on the boundary $\partial\Omega$, while the modelling domain Ω where light scattering occurs is source-free and given by,

$$\nabla \times (\bar{\boldsymbol{\mu}}_r^{-1}\nabla \times \boldsymbol{E}) - k_0^2\bar{\boldsymbol{\epsilon}}_r\boldsymbol{E} = 0. \tag{6}$$

The scattering object is contained in spatial dependent relative permittivity $\bar{\boldsymbol{\epsilon}}_r(\boldsymbol{r})$ and relative permeability $\bar{\boldsymbol{\mu}}_r(\boldsymbol{r})$, and k_0 is vacuum wavenumber. The next step is to test Eq. (6) using test function $\boldsymbol{F}$, which yields the weak form [24,25] of Eq. (6),

$$\int_\Omega d\Omega\{\nabla \times \boldsymbol{F} \cdot \bar{\boldsymbol{\mu}}_r^{-1}\nabla \times \boldsymbol{E} - k_0^2\boldsymbol{F} \cdot \bar{\boldsymbol{\epsilon}}_r\boldsymbol{E}\} - \oint_S \boldsymbol{F} \cdot \hat{\boldsymbol{n}} \times \bar{\boldsymbol{\mu}}_r^{-1}\nabla \times \boldsymbol{E}ds = 0, \tag{7}$$

where the first term of Eq. (7) corresponds to the contribution from volume integral, the second term accounts for the various contributions from the boundaries, such as the numerical ports for the excitation (absorption) from the in-coming (out-going) light wave. As shown in Fig. 1(a), only perfect electric conductor (PEC) boundary conditions and ports are concerned for simplicity. As for PEC boundary condition, the corresponding contribution in Eq. (7) vanishes. Therefore, the boundary contribution in Eq. (7) is simplified as the integral on the ports,

$$\int_\Omega d\Omega\{\nabla \times \boldsymbol{F} \cdot \bar{\boldsymbol{\mu}}_r^{-1}\nabla \times \boldsymbol{E} - k_0^2\boldsymbol{F} \cdot \bar{\boldsymbol{\epsilon}}_r\boldsymbol{E}\} - \sum_{k=1}^{N}\int_{S_k} \boldsymbol{F}_k \cdot \hat{\boldsymbol{n}} \times \bar{\boldsymbol{\mu}}_r^{-1}\nabla \times \boldsymbol{E}_{wg}^{(k)}ds = 0, \tag{8}$$

where $\boldsymbol{E}_{wg}^{(k)}$ is just the superposition of eigen-solutions as given in Eq. (1). In Eq. (8), the surface integral implicitly accounts for the continuity condition of the tangential magnetic field on the ports. Beside, the field continuity condition of the tangential electric field also needs to be taken

Optics EXPRESS

into account. Accordingly, the weak form of continuity condition of electric field can be given as,

$$\int_{S_k} \boldsymbol{F}_k \cdot \hat{\boldsymbol{n}} \times \boldsymbol{E} \times \hat{\boldsymbol{n}} ds = \int_{S_k} \boldsymbol{F}_k \cdot \hat{\boldsymbol{n}} \times \boldsymbol{E}_{wg}^{(k)} \times \hat{\boldsymbol{n}} ds, \tag{9}$$

where the tangential components of the test function on the port, $\boldsymbol{F}_k$, is usually chosen according to the existing symmetry associated with the ports. In photonic devices with Hermitian ports, where time reversal symmetry exist, the test function on the port is chosen as the time reversal symmetry partner of waveguide mode $\boldsymbol{E}_{wg}^{(k)}$, i.e., $\boldsymbol{F}_{k,E} = \boldsymbol{E}_{wg}^{(k),*}$ for electric field. As for non-Hermitian ports, the time reversal symmetry apparently does not hold. However, if the material tensor associated with waveguide on the ports is isotropic, the chiral symmetry is actually valid, and can be used to find the proper test function. Explicitly, the chiral symmetry essentially maps the forward propagating mode into the backward propagating mode, leading to the following choice of the test function on the non-Hermitian port, i.e., $\boldsymbol{F}_{k,E} = \boldsymbol{E}_{wg}^{(k)}$ for electric field, see details in Xiong's work [22]. In relation to the practical implementation, we summarize the detailed comparisons between the Hermitian port and non-Hermitian port for completeness and self-consistency, see Appendix A.

3. Results and discussions

3.1. Light transmission in waveguide lattices

In the following, we investigate the light transmission in one-dimensional dimerized $\mathcal{PT}$-symmetric waveguide lattices. In particular, we demonstrate how the non-Hermitian port implemented in finite element simulation can be used in modelling the scattering behavior in non-Hermitian photonic settings, as well as the relevance of modal orthogonality in extracting S-parameters. As sketched in Fig. 2(a), the first example we consider here is a $\mathcal{PT}$-symmetric waveguide lattice propagating along the x-axis. Each unit cell consists of two geometrically identical waveguides (width $t = 0.1\lambda_0$), with distance $d = 0.7\lambda_0$ and lattice constant $D = \lambda_0$, λ_0 vacuum wavelength. In the dimerized waveguide lattice, the relative permittivity of the waveguide with gain/loss (marked in blue/red) is $\epsilon_r = 10 \pm i\epsilon_i$, where ϵ_i represents the strength of non-Hermiticity. For simplicity, we study numerically the light propagation (along the x-axis) inside single unit cell by taking advantage of periodic boundary condition along the y-axis, as shown in Fig. 2(b), where port 1 and 2 (3 and 4) on the left (right). As the non-Hermiticity is not large, i.e., the value of ϵ_i is small, the structure is still $\mathcal{PT}$-symmetric, where the eigenmodes on both left and right ports are a pair of super-modes with real modal indices. To be specific, the symmetric and antisymmetric super-mode on the left (right) ports are taken as port 1 and 2 (3 and 4), respectively. In contrast with parallel waveguides shown in Fig. 2(b), the unit cell in the second example, see Fig. 2(d), includes two unparallel waveguides with d decreased gradually from $0.7\lambda_0$ to $0.3\lambda_0$. In addition, the distance d between two waveguides in Figs. 2(d) and 2(e) on the left boundary plus that on the right boundary equals to the lattice constant D. All the rest of other settings are the same as those in the first example.

In the first example with $\epsilon_i = 0.1$, Figs. 2(b) and 2(c) present the field amplitude of light propagating from left to right using Hermitian and non-Hermitian port settings respectively. The excitation is imposed on port 1 with symmetric modal profile, while the 'sink' boundary condition on ports 3 and 4 is implemented on the right. In Fig. 2(b), the Hermitian port on the right obviously give rises to reflection, as evident the pattern of the standing waves. In sharp contrast, the proposed non-Hermitian port absorbs right-propagating wave 100% as shown in Fig. 2(c). In the second example for unparallel waveguides with $\epsilon_i = 0.1$, see Fig. 2(d) with Hermitian port and Fig. 2(e) with non-Hermitian port, the distance of the two waveguides varies gradually, leading to the modified modal indices of two supermodes. Figures 2(f) and 2(g) show the modal indices as a function of waveguide distance d. It is worthy to point out that waveguide distance

Optics EXPRESS

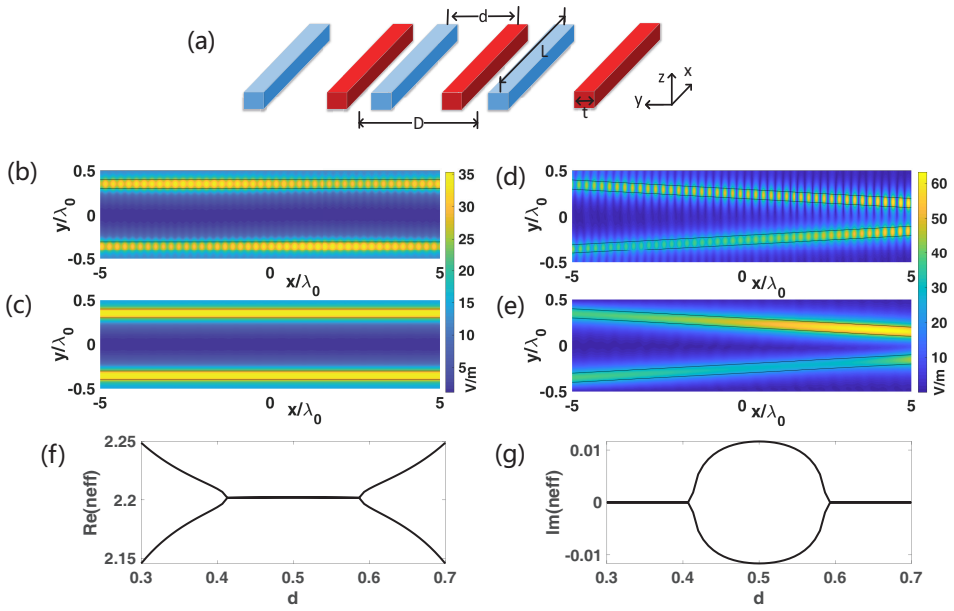

Fig. 2. (a) The schematic diagram of a parallel waveguide lattice, and the red and blue waveguides correspond to those with gain and losses respectively. (b) Result of parallel waveguide lattice via Hermitian port. (c) Field amplitude of parallel waveguide lattice via non-Hermitian port. (d) Field amplitude of unparallel waveguide lattice via Hermitian port. (e) Result of unparallel waveguide lattice via non-Hermitian port. (f) Real part of the modal index as a function of distance d. (g) Imaginary part of effective mode index as a function of distance d.

d is a periodic function of propagation distance x. Apparently, there are three $\mathcal{PT}$-symmetric phases (the first unbroken phase with $d \in [0.3, 0.4]$, broken phase with $d \in [0.4, 0.6]$ and the second unbroken phase with $d \in [0.6, 0.7]$) as d varies, separated by two exceptional points with $d = 0.4$ and $d = 0.6$ respectively. For such complicated modal evolution, it is interesting to see whether the Hermitian port and non-Hermitian port can absorb light completely under the adiabatic approximation. Evidently, the Hermitian port in Figs. 2(d) gives rise to significant artificial reflection, while non-Hermitian port proposed in this paper shown in Figs. 2(e) does not, which unambiguously shows that our non-Hermitian port indeed works very well.

We further study the robustness of the non-Hermitian port from the numerically extracted S-parameters by using the proposed non-Hermitian port. Figure 3 shows the differences of S parameters between Hermitian and non-Hermitian port, as ϵ_i varies from 0 to 0.35. For the parallel waveguide lattice, the exact $\mathcal{PT}$-symmetry is maintained in the whole range of ϵ_i, rendering real values of the propagation constant. Thus, the incident light propagates without gain or losses. As shown in Figs. 3(a) and 3(b), under non-Hermitian port setting (blue line $|S_{31}|$ and asterisk $|S_{13}|$), the sum of $|S_{31}|^2$ and $|S_{11}|^2$ equals to 1, and both $|S_{11}|$ and $|S_{33}|$ are 0, which is consistent with the principle of power conservation in the $\mathcal{PT}$-symmetric phase. In contrast, for the Hermitian port settings, the calculated S-parameters (yellow line $|S_{31}|$ and circle $|S_{13}|$) apparently violates the power conversation, i.e., $|S_{31}|^2 + |S_{11}|^2 > 1$, and the total output power increases for larger ϵ_i. The similar results for unparallel waveguide lattice are shown in Figs. 3(c) and 3(d). Due to the fact that the coupling strength between the two isolated waveguide modes inside the unit cell is the weakest at the middle of the structure, the exact $\mathcal{PT}$ symmetry is broken at $\epsilon_i = 0.06$, which separates the whole region of ϵ_i into two parts, i.e., one (white region)

Optics EXPRESS

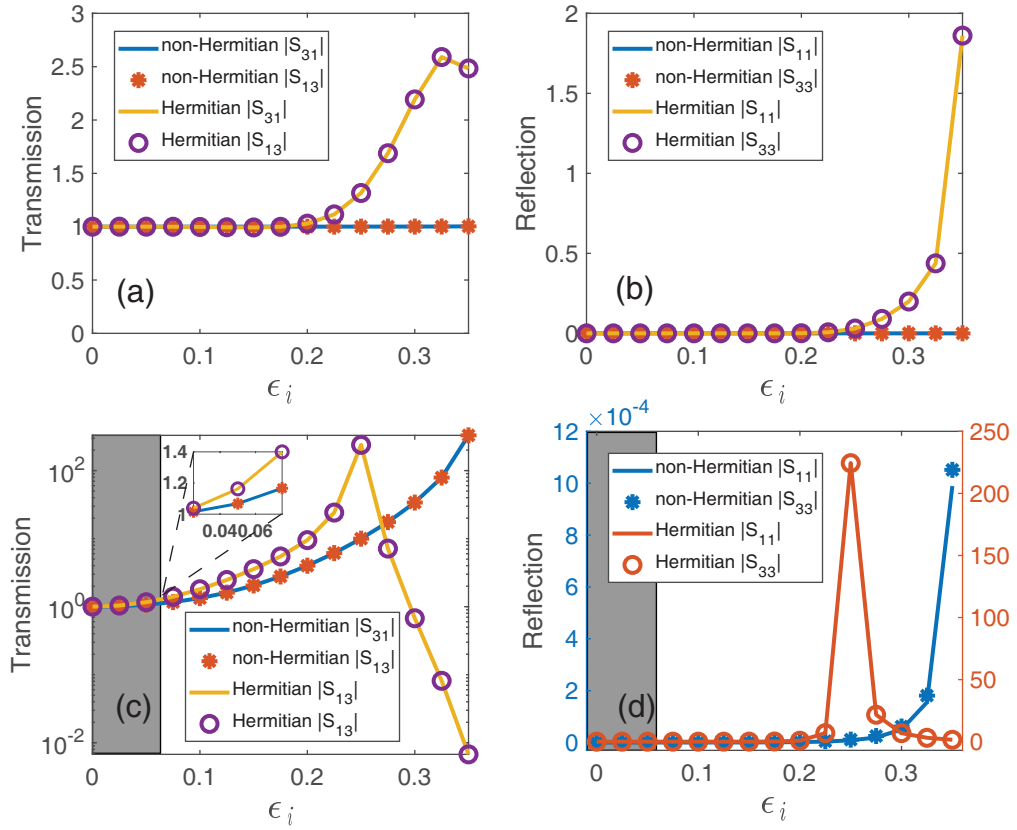

Fig. 3. (a) S_{31} and S_{13} obtained from Hermitian port and non-Hermitian port; (b) S_{11} and S_{22} obtained from Hermitian port and non-Hermitian port; (c) S_{13} and S_{31} obtained from Hermitian port and non-Hermitian port; (d) S_{11} and S_{22} obtained from Hermitian port and non-Hermitian port.

contains EPs, the other (gray region) does not. Actually, the white region corresponds to the situation where modal evolution in the unparallel waveguide lattice encounters the EP twice as light propagates along the x-axis from left to right. In the gray region of Fig. 3(c), the power conservation is preserved due to the presence of exact $\mathcal{PT}$-symmetry during light propagation, i.e., unitary transmission with $|S_{31}| = 1$ ($|S_{13}| = 1$). Indeed, the calculated transmission from non-Hermitian port is nearly 1, while the value obtained from Hermitian port is largely deviated, see inset in Fig. 3(c). In the white region of Fig. 3(c), i.e., $\epsilon_i > 0.06$, light propagates through two regions, i.e., $\mathcal{PT}$ symmetry phase with unitary transmission, $\mathcal{PT}$-symmetry broken phase with amplified amplitude. Evidently, the transmission increases as ϵ_i becomes larger for the non-Hermitian port, see Fig. 3(c), due to the longer amplification region of the light propagation in the $\mathcal{PT}$-symmetry broken phase. In this regard, the non-Hermitian port captures the increasing feature of $|S_{31}|(|S_{13}|)$ as ϵ_i increases, while Hermitian port fails again. Moreover, as shown in Fig. 3(d), the non-Hermitian port gives rise to the full transmission i.e., $|S_{11}|\,(|S_{33}|) = 0$, due to adiabaticity. In contrast, the Hermitian port (orange line for S_{11}, orange circle for S_{33}) gives rise to artificial reflection. In summary, the calculated S-parameters from non-Hermitian port is physical, which is not true for the results obtained from the Hermitian port.

Optics EXPRESS

3.2. Symmetry properties of scattering matrix: numerical verification

Considering the aforementioned waveguide lattices, including the parallel and unparallel lattice, the geometric configurations as well as the material properties associated with the waveguide lattices preserve certain symmetry, i.e., reciprocity and $\mathcal{PT}$-symmetry. Therefore, it is interesting and relevant to see whether those symmetry could impact on the scattering matrix. Indeed, reciprocity requires the scattering matrix $\bar{\boldsymbol{S}}$ to be symmetric [26],

$$\bar{\boldsymbol{S}} = \bar{\boldsymbol{S}}^T, \tag{10}$$

while the $\mathcal{PT}$-symmetry requires that the scattering matrix $\bar{\boldsymbol{S}}$ fulfills the following constraint [6],

$$\mathcal{PT}\bar{\boldsymbol{S}}\mathcal{PT} = \bar{\boldsymbol{S}}^{-1}. \tag{11}$$

Therefore, one can use Eq. (10) and Eq. (11) to identify the symmetry properties of the scattering matrix obtained using our non-Hermitian port, and thus validate the proposed non-Hermitian port from symmetry constraints imposed by reciprocity and $\mathcal{PT}$-symmetry. To that end, we reformulate the 4×4 scattering matrix $\bar{\boldsymbol{S}}$ into 2×2 block matrices, $\bar{\boldsymbol{S}} = \begin{pmatrix} \bar{\boldsymbol{r}} & \bar{\boldsymbol{t}}' \\ \bar{\boldsymbol{t}} & \bar{\boldsymbol{r}}' \end{pmatrix}$, where $\bar{\boldsymbol{r}}$, $\bar{\boldsymbol{r}}'$, $\bar{\boldsymbol{t}}$ and $\bar{\boldsymbol{t}}'$ are 2x2 matrices. As a concrete example, the scattering matrix $\bar{\boldsymbol{S}}$ extracted from unparallel waveguide lattice shown in Fig. 2(e) (the same $\epsilon_i = 0.1$ as that in Figs. 3(c) and 3(d)), is given by $\bar{\boldsymbol{r}} = \bar{\boldsymbol{0}}$, $\bar{\boldsymbol{r}}' = \bar{\boldsymbol{0}}$, $\bar{\boldsymbol{t}} = \begin{bmatrix} 0.59+0.99i & -0.58+0.33i \\ -0.58+0.33i & 0.48-1.05i \end{bmatrix}$, $\bar{\boldsymbol{t}}' = \begin{bmatrix} 0.59+0.99i & -0.58+0.33i \\ -0.58+0.33i & 0.48-1.05i \end{bmatrix}$. Here the time-reversal operator $\mathcal{T}$ is simply a complex conjugate and the parity operator $\mathcal{P}$ can be presented as a matrix form, $\mathcal{P}$ = diag[1, -1, 1, -1]. Importantly, the numerically extracted scattering matrix $\bar{\boldsymbol{S}}$ satisfies the constraints imposed by reciprocity and $\mathcal{PT}$-symmetry. We find that symmetric constraints imposed by reciprocity and $\mathcal{PT}$-symmetry can be satisfied in the whole range of ϵ_i (not shown here) or other geometric configurations of waveguide lattices, not limited at the special value $\epsilon_i = 0.1$, nor the particular waveguide lattice shown in Fig. 2(e).

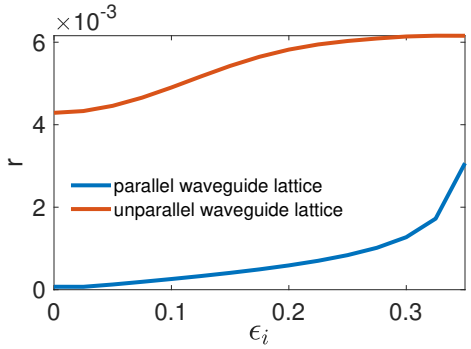

Fig. 4. The relative error of the $\mathcal{PT}$-symmetry constraint.

Lastly, we examine the relative error r, i.e., $r = \frac{\mathcal{P}S^*\mathcal{P}-S^{-1}}{|||S|||_{\max}}$ and $|||S|||_{\max} = \max\{|S_{ij}|\}$, as a function of ϵ_i in Fig. 4. Evidently, we find that the maximum relative error r for either the parallel waveguide lattice or unparallel waveguide lattice, is less than 1%, which can be considered as reasonably accurate results. Briefly, the symmetry considerations as well as relatively accurate results indicate the strength of our proposed non-Hermitian ports that might readily be useful for the modelling of non-Hermitian photonic devices.

Optics EXPRESS

4. Conclusions

In summary, we develop the concept of non-Hermitian ports that work reasonably well in the waveguide port containing gain and losses. In our model, the modal orthogonality on the non-Hermitian ports is restored using bi-orthogonal inner product, and the finite element implementation of non-Hermitian port is realized using similar procedures as those of the conventional ports, i.e., tangential field continuity of electric and magnetic fields, but with carefully chosen test function and normalization condition that are consistent with the bi-orthogonal inner product. We further use our non-Hermitian port to numerically extract the scattering matrices from two different $\mathcal{PT}$-symmetric waveguide lattices and compare the results with those obtained from Hermitian port. The comparison shows strong evidence that the scattering matrices from our non-Hermitian port are physical. In contrast, the scattering matrices from the conventional Hermitian port yields unphysical results. We further examine the constraints imposed by the existing symmetry associated with the waveguide lattice onto the scattering matrix, and find that our numerically extracted scattering matrices indeed reflect reciprocity and $\mathcal{PT}$ symmetry of the waveguide lattice, which can be seen as a further evidence that our non-Hermitian port can be used to model the non-Hermitian photonic devices. Lastly, we study the relative error (the maximum is less than 1%) of our numerical realization of non-Hermitian port by taking advantage of the symmetry properties of the scattering matrix, showing that the proposed non-Hermitian port is reasonably accurate.

Appendix A: practical implementation of Hermitian port and non-Hermitian port in finite element method

Table 1. Extracting the scattering matrix element S_{1j} for Hermitian and non-Hermitian port

		Hermitian	non-Hermitian
Normalization		$P = \frac{1}{2} real(\iint t\vec{E}_0 \times t\vec{H}_0^* dxdy)$	$P = \frac{1}{2} \iint t\vec{E}_0 \times t\vec{H}_0 dxdy$
		$t\vec{E}_1(t\vec{H}_1) = t\vec{E}_0(t\vec{H}_0)\sqrt{\left\|\frac{P_{in}}{P}\right\|}$	$t\vec{E}_1(t\vec{H}_1) = t\vec{E}_0(t\vec{H}_0)\sqrt{\frac{P_{in}}{P}}$
Continuity condition of $\boldsymbol{H}$ field	Weak Expression	$\iint test(on + S_{1j}) \cdot t\vec{E}_1^* \cdot i\omega\mu_0 (-\vec{n} \times t\vec{H}_1)(S_{1j} - on)dxdy = 0$	$\iint test(on + S_{1j}) \cdot t\vec{E}_1 \cdot i\omega\mu_0 (-\vec{n} \times t\vec{H}_1)(S_{1j} - on)dxdy = 0$
Continuity condition of $\boldsymbol{E}$ field	Constraint	$t\vec{E} = (on + S_{1j})t\vec{E}_1$	
	Constraint force	$test(t\vec{E}) = test((on + S_{1j}) \cdot t\vec{E}_1^*)$	$test(t\vec{E}) = test((on + S_{1j}) \cdot t\vec{E}_1)$

Table 1 shows the practical implementation of ports for Hermitian and non-Hermitian settings in finite element method with the target to calculate S-parameter S_{1j}, which refers to the scenario with excitation on port j but detection on port 1. In Table 1, $t\vec{E}_0/t\vec{H}_0$ is the tangential electric/magnetic field of the waveguide mode on the port calculated directly from mode solver, $t\vec{E}_1/t\vec{H}_1$ is the normalized tangential electric and magnetic field of waveguide mode, and S_{1j} as well as $t\vec{E}$ (tangential electric field of dependent variable $\vec{E}$) are the dependent variables which need to be determined. Since $t\vec{E}_0$ ($t\vec{H}_0$) are calculated from the mode solver, the prescribed modal profile on the port requires that $t\vec{E}_0$ ($t\vec{H}_0$) needs to be normalized properly. In Hermitian waveguide, the normalized factor simply is taken as the time-averaged power on the cross section of the port, while for non-Hermitian port the normalized factor needs to be calculated using bi-orthogonal inner product, as tabulated in the first row of Table 1. Subsequently, the continuity condition of the electric and magnetic field needs to be realized: (1) the continuity of magnetic field is taken into account via the boundary term contribution to the weak form (Eq. (7)), see the

Optics EXPRESS

second row in Table.1; (2) the continuity of electric field is realized by introducing the auxiliary equations, i.e., $t\vec{E} = (on + S_{1j})t\vec{E}_1$, which are implemented numerically using the conditions of constraint and constraint force, given by the third row in Table 1. In Table 1, the term *on* is equal to 1 if j =1, otherwise *on*=0.

Funding

National Natural Science Foundation of China (NSFC) (11874026, 61735006, 61775063); Fundamental Research Funds for the Central Universities (HUST) (2017KFYXJJ027); National Key Research and Development Program of China (2017YFA0305200).

References

1. D. M. Pozar, *Microwave Engineering* (John Wiley & Sons, 2009).
2. L. A. Coldren, S. W. Corzine, and M. L. Mashanovitch, *Diode Lasers and Photonic Integrated Circuits* (John Wiley & Sons, 2012).
3. J. Xu and Y. Chen, "General coupled mode theory in non-Hermitian waveguides," Opt. Express **23**, 22619–22627 (2015).
4. B. Wu, B. Wu, J. Xu, J. Xiao, and Y. Chen, "Coupled mode theory in non-Hermitian optical cavities," Opt. Express **24**, 16566–16573 (2016).
5. X. Zhu, H. Ramezani, C. Shi, J. Zhu, and X. Zhang, "$\mathcal{PT}$-Symmetric Acoustics," Phys. Rev. X **4**, 031042 (2014).
6. Y. D. Chong, L. Ge, and A. D. Stone, "$\mathcal{PT}$-Symmetry Breaking and Laser-Absorber Modes in Optical Scattering Systems," Phys. Rev. Lett. **106**, 093902 (2011).
7. L. Ge, Y. D. Chong, and A. D. Stone, "Conservation relations and anisotropic transmission resonances in one-dimensional $\mathcal{PT}$-symmetric photonic heterostructures," Phys. Rev. A **85**, 023802 (2012).
8. L. Ge, K. G. Makris, D. N. Christodoulides, and L. Feng, "Scattering in $\mathcal{PT}-$ and $\mathcal{RT}$-symmetric multimode waveguides: Generalized conservation laws and spontaneous symmetry breaking beyond one dimension," Phys. Rev. A **92**, 062135 (2015).
9. T. Liu, X. Zhu, F. Chen, S. Liang, and J. Zhu, "Unidirectional Wave Vector Manipulation in Two-Dimensional Space with an All Passive Acoustic Parity-Time-Symmetric Metamaterials Crystal," Phys. Rev. Lett. **120**, 124502 (2018).
10. X.-F. Zhu, "Defect states and exceptional point splitting in the band gaps of one-dimensional parity-time lattices," Opt. Express **23**, 22274–22284 (2015).
11. X.-F. Zhu, Y.-G. Peng, and D.-G. Zhao, "Anisotropic reflection oscillation in periodic multilayer structures of parity-time symmetry," Opt. Express **22**, 18401–18411 (2014).
12. Y. D. Chong, L. Ge, H. Cao, and A. D. Stone, "Coherent Perfect Absorbers: Time-Reversed Lasers," Phys. Rev. Lett. **105**, 053901 (2010).
13. S. Longhi, "$\mathcal{PT}$-symmetric laser absorber," Phys. Rev. A **82**, 031801 (2010).
14. M. G. Silveirinha, "$\mathcal{P} \cdot \mathcal{T} \cdot \mathcal{D}$ symmetry-protected scattering anomaly in optics," Phys. Rev. B **95**, 035153 (2017).
15. J. Doppler, A. A. Mailybaev, J. Böhm, U. Kuhl, A. Girschik, F. Libisch, T. J. Milburn, P. Rabl, N. Moiseyev, and S. Rotter, "Dynamically encircling an exceptional point for asymmetric mode switching," Nature **537**, 76 (2016).
16. X.-L. Zhang, S. Wang, B. Hou, and C. T. Chan, "Dynamically Encircling Exceptional Points: In situ Control of Encircling Loops and the Role of the Starting Point," Phys. Rev. X **8**, 021066 (2018).
17. K. X. Wang, "Time-reversal symmetry in temporal coupled-mode theory and nonreciprocal device applications," Opt. Lett. **43**, 5623–5626 (2018).
18. F. Shanhui, S. Wonjoo, and J. D. Joannopoulos, "Temporal coupled-mode theory for the Fano resonance in optical resonators," J. Opt. Soc. Am. A **20**, 569–572 (2003).
19. W. Chen, Z. Xiong, J. Xu, and Y. Chen, "Generalized coupled mode formalism in reciprocal waveguides with gain/loss, anisotropy or bianisotropy," arXiv preprint arXiv:1801.06673 (2018).
20. E. Silvestre, M. A. Abián, B. Gimeno, A. Ferrando, M. V. Andrés, and V. E. Boria, "Analysis of inhomogeneously filled waveguides using a bi-orthonormal-basis method," IEEE Trans. Microw. Theory Tech. **48**, 589–596 (2000).
21. A. W. Snyder and J. Love, *Optical Waveguide Theory* (Springer Science & Business Media, 2012).
22. Z. Xiong, W. Chen, P. Wang, and Y. Chen, "Classification of symmetry properties of waveguide modes in presence of gain/losses, anisotropy/bianisotropy, or continuous/discrete rotational symmetry," Opt. Express **25**, 29822–29834 (2017).
23. http://www.comsol.com/.
24. O. C. Zienkiewicz, R. L. Taylor, O. C. Zienkiewicz, and R. L. Taylor, *The Finite Element Method* (McGraw-Hill London, 1977).
25. G. Pelosi, R. Coccioli, and S. Selleri, *Quick Finite Elements for Electromagnetic Waves* (Artech House, 2009).
26. D. Jalas, A. Petrov, M. Eich, W. Freude, S. Fan, Z. Yu, R. Baets, M. Popović, A. Melloni, J. D. Joannopoulos, M. Vanwolleghem, C. R. Doerr, and H. Renner, "What is – and what is not – an optical isolator," Nat. Photonics **7**, 579–582 (2013).